J. Fluid Mech. (1992), *vol.* 245, *pp.* 599–617

Comparison between rough- and smooth-wall turbulent boundary layers

By P.-Å. KROGSTAD[1], R. A. ANTONIA[2] AND L. W. B. BROWNE[2]

[1] Division of Hydro- and Gas Dynamics, Norwegian Institute of Technology, Trondheim, 7034, Norway

[2] Department of Mechanical Engineering, University of Newcastle, NSW, 2308, Australia

(Received 7 June 1991 and in revised form 1 April 1992)

Measurements in a zero-pressure-gradient turbulent boundary layer over a mesh-screen rough wall indicate several differences, in both inner and outer regions, in comparison to a smooth-wall boundary layer. The mean velocity distribution indicates that, apart from the expected k-type roughness function shift in the inner region, the strength of the rough-wall outer region 'wake' is larger than on a smooth wall. Normalizing on the wall shear stress, there is a significant increase in the normal turbulence intensity and a moderate increase in the Reynolds shear stress over the rough wall. The longitudinal turbulence intensity distribution is essentially the same for both surfaces. Normalized contributions to the Reynolds shear stress from the second (Q2) and fourth (Q4) quadrants are greater over the rough wall. The data indicate that not only are Q2 and Q4 events stronger on the rough wall but their frequency of occurrence is nearly twice as large for the rough wall as for the smooth wall. Comparison between smooth- and rough-wall spectra of the normal velocity fluctuation suggests that the strength of the active motion may depend on the nature of the surface.

1. Introduction

Significant attention has been given to the study of the structure of a zero-pressure-gradient boundary layer over a smooth wall. The data, collected mainly via experiments and, more recently, through direct numerical simulations have ranged from distributions of conventional Reynolds stresses (e.g. Klebanoff 1955) to information associated with various aspects of the organized motion (e.g. Kline & Robinson 1990). Measurements of several turbulence quantities (both conventional and conditional) have also been made in zero-pressure-gradient turbulent boundary layers over various types of surface roughness. While some attention has been given to the turbulence structure over rough walls (e.g. the hydrogen bubble investigation of Grass 1971), it is reasonable to assert that our knowledge of this structure is less detailed than for a smooth wall.

In a recent review of rough-wall turbulent boundary layers, Raupach, Antonia & Rajagopalan (1991) considered both two-dimensional and three-dimensional laboratory rough surfaces as well as natural vegetated surfaces in the atmosphere. The effect of the roughness on the mean velocity appears to be fairly well documented and understood. With regard to the effect of the roughness on turbulence intensities, the review examined Townsend's (1976) Reynolds-number similarity hypothesis as

modified slightly by Perry & Abell (1977). In the context of rough-wall boundary layers, the hypothesis (labelled 'wall similarity hypothesis') states that, outside the roughness sublayer (a region influenced by lengthscales associated with the roughness elements and extending to about five times the roughness height k), turbulent motions are independent of the wall roughness at sufficiently large Reynolds numbers. With the qualification that measurement errors (especially in the use of $\times$-probes near rough surfaces, e.g. Perry, Lim & Henbest 1987) may be important, the weight of the available experimental evidence indicates fairly strong (though not unanimous) support for the hypothesis. One implication of this hypothesis is that outside the roughness sublayer (or viscous sublayer for a smooth wall) distributions of turbulence intensities normalized using the wall shear stress should be essentially the same over smooth and rough surfaces. More generally, the turbulence structure over a significant part of the layer should be unchanged in spite of significant alterations to the wall. This perspective would imply even less communication between the wall region and the outer region of a boundary layer than may be normally assumed.

The present investigation was initiated mainly with a view to provide a topological study of the large-scale motion over a rough surface with at least the same degree of detail as previously obtained for a smooth surface (Antonia, Bisset & Browne 1990). Prior to determining the topology, the mean velocity and turbulence characteristics of the rough-wall boundary layer were obtained using a Pitot tube, single hot wires and $\times$-wire probes. Special attention was given to the possible errors associated with $\times$-wire measurements, resulting in the use of several $\times$-probe geometries. During the course of this investigation, it became evident that, outside the roughness sublayer, the statistics of v, the velocity fluctuation normal to the wall, differed significantly from those measured in a smooth-wall boundary layer (at a sufficiently large Reynolds number for Reynolds-number similarity to apply). The present paper documents these differences and discusses them in the context of previous rough-wall measurements and the wall similarity hypothesis. The differences have also been explored in terms of contributions to the Reynolds shear stress from quadrants 2 and 4 of the (u, v)-plane and in the context of spectra of the velocity fluctuations. The topology-related results will be presented at a later stage.

2. Experimental details

The experiments were carried out in an open-return blower tunnel with a rectangular test section. The test section was 5.4 m long with an aspect ratio of 5.8:1 at the start where the width was 152 mm. The width of the test section was adjusted to compensate for the boundary-layer growth so that the static pressure was kept constant within $\pm 0.24\%$ of the reference dynamic head along the 3.5 m where data were taken. Complete details for the rough-wall experiment may be found in Krogstad & Browne (1991) while the smooth-wall data have been described in Antonia *et al.* (1990).

The boundary layer was tripped at the exit of the contraction using a 4 mm trip rod that spanned the entire test section, followed by a 15 cm wide strip of no. 40 grit sandpaper. It was verified by Antonia *et al.* (1990) that the boundary layer produced behaved according to the criteria for fully developed turbulent boundary layers. For the experiments on the rough surface, one tunnel wall was covered with a stainless steel woven mesh screen inserted immediately downstream of the trip device. This mesh was made of 0.69 mm wires with 3.18 mm centreline spacing giving an openness

of 61%. The thickness of the screen was $k = 1.55$ mm, i.e. somewhat larger than twice the wire diameter. The ratio of centreline spacing to wire diameter was thus 4.61. According to the study of Furuya & Fujita (1967), this is a mesh geometry which gives the largest roughness effect, i.e. the largest magnitude of the roughness function $\Delta\bar{U}^+$ (defined in (1)), for a given wire diameter.

The mesh extended 3.53 m downstream from the trip and spanned the entire test section. Small drops of epoxy glue were applied (over approximately a 40 mm square grid) to ensure that the screen was laid flat against the aluminium base surface.

Mean velocity profiles were obtained at a number of streamwise positions along the centreline using a Pitot tube of 1.25 mm diameter and a number of single-wire and $\times$-wire probes of different geometries. The wires were etched from Platinum–10% Rhodium Wollaston wires ranging from $d_w = 1.3$ to 5 μm. The majority of the measurements were made with $d_w = 2.5$ μm. The $\times$-wires were calibrated using the effective angle approach. This is described in Browne, Antonia & Chua (1989*a*) where the method is compared with a full velocity *vs.* yaw-angle calibration technique and shown to give comparable results even where the turbulence intensities are high. Probes with wires crossing at 120° were used, for reasons outlined in Browne, Antonia & Chua (1989*b*). Velocity calibration involved fitting a least-squares fourth-order polynomial to the velocity *vs.* voltage data. Subsequent data reduction used the effective angles and polynomial fits. The hot-wire drift was monitored by moving the probe to a reference station outside the boundary layer at regular intervals. If the total drift during a traverse was more than 1% the data set was rejected. Using this procedure it was found, when compiling 13 sets of data (one with the Pitot tube, five with single wires and seven with $\times$-wires), that the mean velocities agreed to within $\pm 0.7\%$ throughout the boundary layer.

Most of the measurements were taken at $x = 2.46$ m at a free-stream velocity of $U_e = 20$ m/s. Under these conditions, the Reynolds number based on the momentum thickness, θ, was $Re_\theta = 12800$ with a boundary-layer thickness of $\delta = 75$ mm.

Using single hot wires, the dissipation rate was estimated by assuming local isotropy and Taylor's hypothesis. The Kolmogorov lengthscale, $\eta = (\nu^3/\epsilon)^{\frac{1}{4}}$, increased from about 0.06 mm close to the wall to about 0.14 mm at $y/\delta \approx 0.5$. The majority of the hot wires used had a sensor length of about $l_w = 0.35$ mm and a length-to-diameter ratio of 140 giving $l_w/\eta \approx 3.5$ for most of the boundary layer. For $d_w = 1.3$ μm, the wire length was only 0.31 mm so that l_w/η was less than 4.5 everywhere in the layer.

Using the estimated distribution of η, the maximum Kolmogorov frequency, $f_k\,(=\bar{U}/2\pi\eta)$ across the layer was about 27 kHz at $y/\delta \approx 0.4$. Since the interest here is not in the fine structure of the turbulence, it was decided, after a preliminary examination of spectra of the hot-wire signals, to use a low-pass filter (−24 dB/octave) with the cutoff frequency set at 10 kHz. The signals were digitized using a RC Electronics 16 channel, 12 bit A/D converter at a sampling frequency of 20 kHz into a NEC 386 personal computer and the digital records (usually 20 s of continuous data) transferred by Ethernet to a VAX 8550 computer for subsequent analysis.

3. Mean velocity profiles

Owing to the higher surface drag on the rough wall, the mean velocity profiles on a rough surface are less full than those obtained on a smooth surface (e.g. figure 1*a*). The higher drag also implies a faster growth rate and therefore greater entrainment of irrotational fluid. Also, for the same nominal free-stream velocity ($U_e = 20$ m/s)

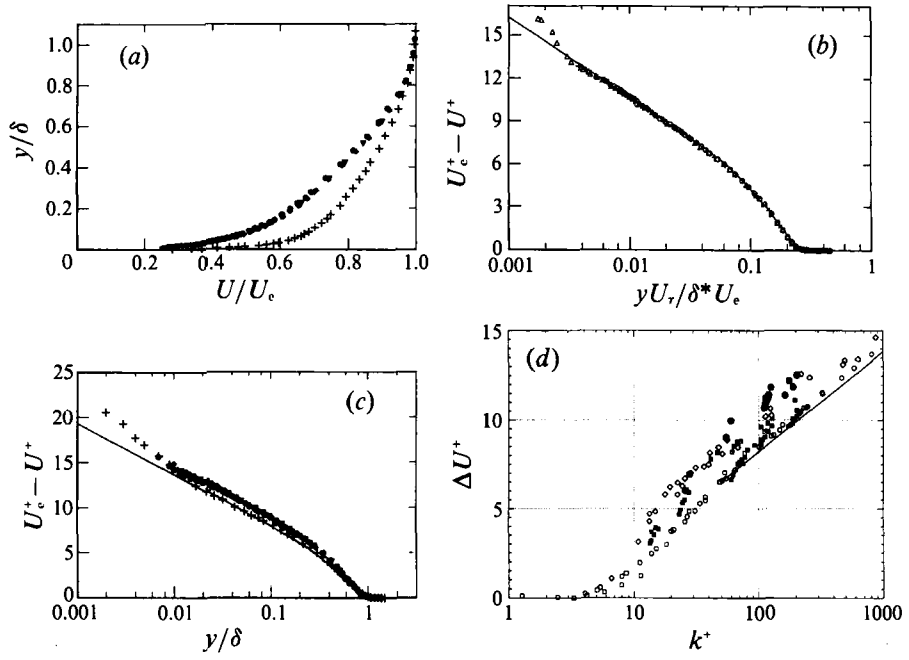

FIGURE 1. Mean velocity distributions on a rough wall and comparison with a smooth wall: (*a*) plotted in physical coordinates; (*b*) velocity-defect plot, data reduced using (3) and (4): ——, Hama (1954); (*c*) velocity-defect plot, data reduced using (1), (2) and (7). Smooth wall: +, $R_\theta = 6500$ (5 μm single wire). Rough wall ($R_\theta = 12800$): △, ●, 2.5 μm single wire; ◆, 1.3 μm, 120° ×-wire with $l/d = 240$; ▼, 2.5 μm, 128° ×-wire with $l/d = 224$. (*d*) Roughness function, $\Delta\bar{U}^+$: ——, Prandtl–Schlichting; □, Colebrook–White uniform sand; ○, Nikuradse uniform sand; ◇, Hama mesh screen; Furuya & Fujita mesh screen, ⊞, $t/d = 3.9$; ⊠, $t/d = 6.0$; ●, present mesh screen, $t/d = 4.61$.

the Reynolds number based on the momentum thickness is much higher for the rough surface ($R_\theta = 12800$) than for the smooth surface ($R_\theta = 6500$). There is general consensus that the major Reynolds-number effects on the mean velocity distribution, at least on a smooth surface, are found for $R_\theta < 3000$. Hence it is expected that the flow is fully developed.

For both surfaces, the mean velocity profile can, very approximately, be thought to comprise two regions. In the inner region, the appropriate velocity scale is the friction velocity U_τ while the appropriate lengthscale is the viscous lengthscale ν/U_τ and the roughness lengthscale k. In the outer region, U_τ remains appropriate, but the characteristic lengthscale is now the boundary-layer thickness δ. Ignoring the viscous sublayer or the roughness sublayer in the rough case, the velocity distribution across these two regions is given by

$$\bar{U}^+ = \frac{1}{\kappa}\ln y^+ + A - \Delta\bar{U}^+ + \frac{2\Pi}{\kappa}\omega(\eta), \tag{1}$$

where $\bar{U}^+ = \bar{U}/U_\tau$, $y^+ = (y+\epsilon)\,U_\tau/\nu$ and $\eta = (y+\epsilon)/\delta$. ϵ is the shift in origin required in the case of a rough wall (here, y is measured from the top of the mesh screen). κ and A are believed to be the same for rough and smooth surfaces, here taken to be 0.41 and 5.3 respectively. $\Delta\bar{U}^+$ is the roughness function (zero for a smooth wall). The parameter Π determines the strength of the wake function $\omega(\eta)$.

Equation (1) indicates that the description of the measured velocity profile in the rough case requires the determination of four parameters: U_τ, ϵ, $\Delta\overline{u}^+$ and Π. This is twice as many as for a smooth-surface boundary layer. It is therefore to be expected that the mean velocity profile may not provide as sensitive a criterion for quantifying the effect of the surface roughness as some of the turbulence quantities. Rewriting this equation in a velocity-defect form, i.e. subtracting $\bar{U}^+$ from its own value at the edge of the boundary layer, simplifies the problem by reducing the number to three, namely

$$U_e^+ - \bar{U} = \frac{2\Pi}{\kappa}[\omega(1) - \omega(\eta)] - \frac{1}{\kappa}\ln\eta \tag{2}$$

since the difference $A - \Delta\bar{U}^+$ vanishes.

Many forms have been proposed for the wake function. A commonly used form for boundary layers on rough surfaces (Furuya & Fujita 1967; Perry *et al.* 1987; Bandyopadhyay 1987) is Hama's (1954) formulation. Hama split (2) into two parts. For small values of η, (2) is dominated by the logarithmic term, and is therefore written

$$U_e^+ - \bar{U}^+ = -\frac{1}{\kappa}\ln\frac{(y+\epsilon)}{\delta^* U_e^+} - 0.6 \quad \text{for} \quad \eta \lesssim 0.15, \tag{3}$$

where $\delta^* U_e^+$ has been used instead of δ as proposed by Clauser (1956). Further out, the wake dominates and Hama proposed for this second part the function

$$U_e^+ - \bar{U}^+ = 9.6(1-\eta)^2 \quad \text{for} \quad \eta \geqslant 0.15. \tag{4}$$

Figure 1 (*b*) shows data reduced using (3) and (4). They are seen to follow Hama's formulation closely. Using this formulation, only U_τ and ϵ need to be determined since the wake strength is fixed implicitly. However, as observed by Perry *et al.* and Bandyopadhyay, the value of U_τ obtained in this way is consistently much higher than values obtained from either a momentum balance or by extrapolating the Reynolds shear stress to the wall. Bradshaw (1987) suggested that this may be due to the strength of the wake, as implied by (4), being too small. The wake is found as the difference between (3) and (4). The largest value in the wake is found at the point in the outer region where the two equations have the same gradient. By defining the strength of the wake at this point as $2\Pi/\kappa$, Π is found to be

$$\Pi = -\tfrac{1}{2}\{\ln\xi_0 + \kappa[9.6(1-\xi_0/B)^2 + 0.6]\}, \tag{5}$$

where ξ_0, the coordinate where the gradients are the same, is given by

$$\xi_0 = \tfrac{1}{2}B[1 + (1 - 1/4.8\kappa)^{\frac{1}{2}}] = 0.85B \tag{6}$$

and $B = \delta/\delta^* U_e^+$. For $B = 0.3$, which was used by Bandyopadhyay, the wake strength is found to be $\Pi = 0.52$. Coles (1956) initially proposed that for zero-pressure-gradient turbulent boundary layers Π would be 0.55 for high Reynolds numbers, but later (1987) gave an asymptotic value of 0.62. Osaka & Mochizuchi (1988) obtained a value of $\Pi = 0.68$ at $R_\theta = 5300$ for a *d*-type rough-surface boundary layer. They commented that the high value reflects the high entrainment rate over a rough wall. Tani (1988), who re-evaluated a number of previously reported results for *k*- and *d*-type surfaces, obtained values of Π ranging from 0.4 to 0.7 for *k*-surfaces and got even higher values for *d*-type roughness. It seems therefore that the fixed value of Π in Hama's formulation may not be optimal for a rough surface.

It was therefore decided to use a formulation that allows Π to be optimized also. The formulation proposed by Finley, Khoo Chong Phoe & Chin Jeck Poh (1966) and later by Granville (1976), namely

$$\omega(\eta) = (1/2\Pi)[(1+6\Pi)-(1+4\Pi)\,\eta]\,\eta^2 \tag{7}$$

was used since it satisfies two boundary conditions (correct slope and function values) both near the wall and at the boundary-layer edge. Using a least-squares optimization technique, (2) and (7) were fitted to the mean velocity profiles to provide values for U_τ, ϵ and Π. In the case of the smooth surface, for which ϵ and $\Delta\bar{U}^+$ are zero, (1) and (7) were used. The optimization is based on the assumption that a function f used to describe a set of data points depends, in general, on a number of constants A_n whose values are to be optimized. The sensitivity of f to changes in these constants, ΔA_n, is then given by

$$\Delta f = \sum \frac{\partial f}{\partial A_n}\Delta A_n. \tag{8}$$

If f and its derivatives with respect to A_n are known, a linear set of equations may be constructed that can be used on a least-squares basis to minimize the difference between the measured data and the function. Unlike the least squares fit of a polynomial, where an exact determination of A_n is possible by direct matrix inversion, the solution to general functions such as (1)–(7) must be obtained by iteration. A nice feature of this method is that since the constants to be found are assumed to be valid all the way through the layer, different formulae containing the constants may be used in different parts of the layer in the same optimization process. This allowed, for example, U_τ to be optimized by using (3) and (4) simultaneously.

Using (2) and (7), f may be written

$$f = \frac{\bar{U}}{U_e} = 1+\frac{U_\tau}{\kappa U_e}\left\{\ln\left(\frac{y+\epsilon}{\delta}\right)-(1+6\Pi)\left[1-\left(\frac{y+\epsilon}{\delta}\right)^2\right]+(1+4\Pi)\left[1-\left(\frac{y+\epsilon}{\delta}\right)^3\right]\right\}. \tag{9}$$

This equation needs to be optimized for $A_n = \Pi$, ϵ and U_τ. The use of (8) gives three nonlinear equations which may be solved for the three A_n.

In figure 1(*c*) rough-wall data reduced in this way as well as a set for the smooth wall have been plotted. Although in close agreement, the smooth- and rough-surface data no longer collapse on to the same line. The smooth-wall data are seen to follow (3) and (4) closely without imposing a specific value of Π. If the deviation from the velocity-defect curve of Hama in the rough case is correct, the results indicate that the velocity profiles for the two surfaces must be different not only in the wall region, but also in the outer part of the boundary layer.

The shift in the log law obtained from the fit is shown in figure 1(*d*). Also included are data from the mesh screen experiments of Hama (1954) and Furuya & Fujita (1967) with slightly different mesh densities. As pointed out in §2 the present mesh geometry was chosen to give the largest shift according to the recommendations of Furuya & Fujita. The figure shows that this has been achieved as the present results gave larger shifts than was obtained by the geometries they used and marginally higher values than those obtained by Hama. Also included are data for sand grain roughness. The figure shows that the results obtained with the present surface are fully consistent with a k-type behaviour.

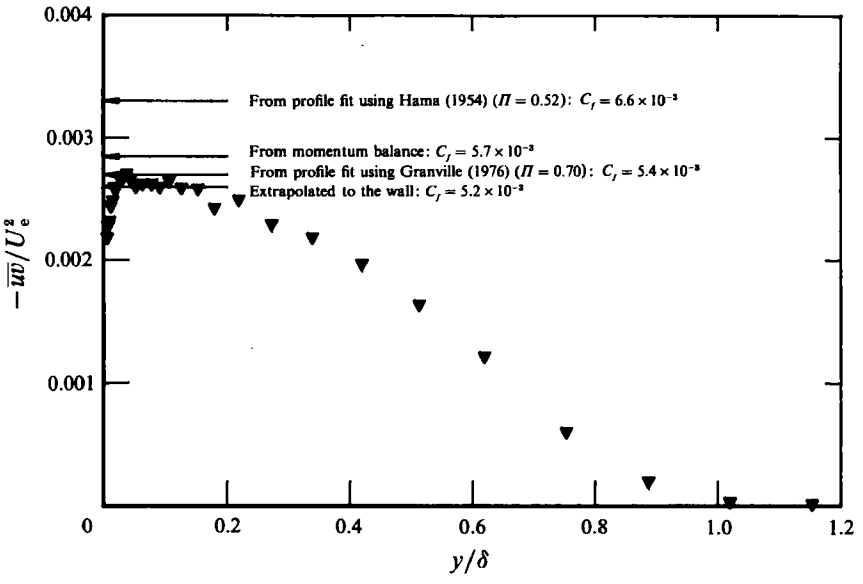

FIGURE 2. Friction velocity obtained from Reynolds shear stress profile (2.5 μm ×-wire with 128° apex angle) and comparison with friction velocity inferred from momentum integral balance and fit to the mean velocity profile.

The average log-law shift at the main measurement station, $x = 2.46$ m, for this surface was found to be $\Delta\bar{U}^+ \approx 11$ at $k^+ = 104$. The equivalent shift for sand-grain type of roughness is (Raupach *et al.* 1991)

$$\Delta\bar{U}^+ = (1/\kappa)\ln k_s^+ - 3.2, \tag{10}$$

from which the equivalent sand roughness for the present mesh is found to be $k_s = 3.2k = 4.96$ mm.

The method used to fit the profiles gave a skin friction coefficient of $C_f = 2.8 \times 10^{-3}$ for the smooth-wall profile. This agrees well with $C_f = 2.9 \times 10^{-3}$ obtained from the Preston tube. Π was found to be 0.51. For the rough wall, $C_f = 5.4 \times 10^{-3}$ and $\Pi = 0.70$. This rather high value of Π is about the same as the value obtained by Osaka & Mochizuki (1988) and Tani *et al.* (1988) for *d*-type rough walls. Figure 2 shows that the skin friction coefficient obtained in the case of the rough wall when Π is allowed to vary is in much better agreement with the wall shear stress obtained by extrapolating the measured Reynolds shear stress to the wall than is the rather high value obtained using the formulation of Hama. It therefore appears that Hama's formulation may only be applied with confidence for smooth-surface boundary layers.

The shift obtained from the fit was $\epsilon/k = 0.25$. However, considerable scatter was found in ϵ. Since it is very difficult to position the probe repeatedly at the same position relative to the irregular rough surface, any positioning error will be reflected in ϵ. Also, since the flow close to the roughness elements changes rapidly in the streamwise and lateral directions, the positioning errors in these directions cause every measured profile to be different close to the surface. Since this is where y and ϵ are comparable, this region influences the value of ϵ strongly. Therefore the data fit was restricted to $y > k$.

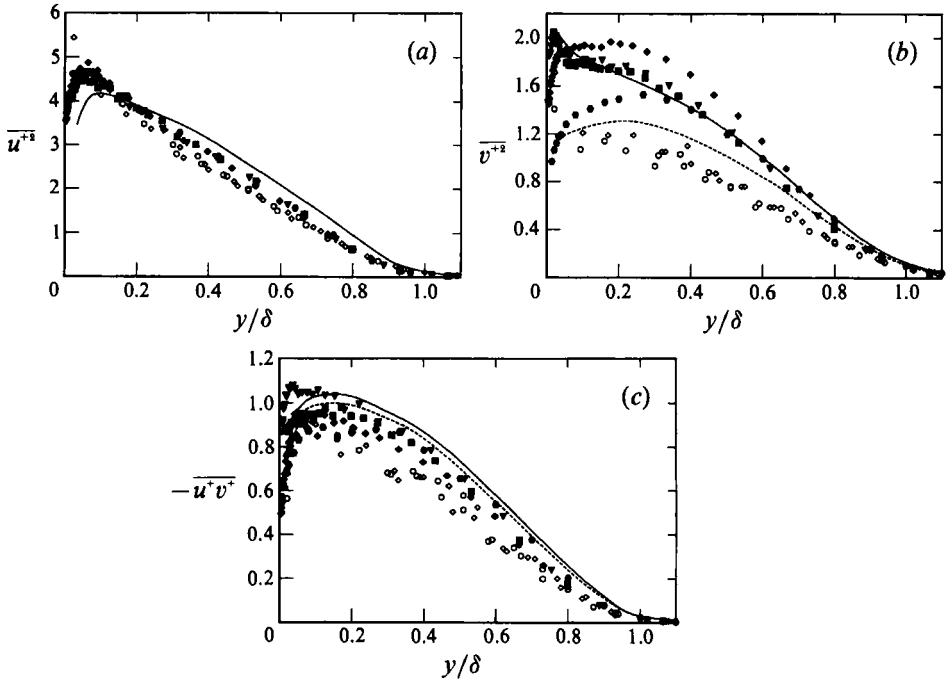

FIGURE 3. Reynolds stresses: (a) $\overline{u^{+2}}$; (b) $\overline{v^{+2}}$; (c) $-\overline{u^+v^+}$. Smooth wall: ◇, $R_\theta = 6030$; ○, 9630 (5 μm, 90° ×-probes with $l/d = 250$); Rough wall: symbols as in figure 1, and ●, 5 μm, 95° ×-wire with $l/d = 140$; ■, 5 μm, 129° ×-wire with $l/d = 140$; ---, Acharya & Escudier (1987) 90° probe; ——, Acharya & Escudier (1987) 120° probe.

4. Reynolds stresses

Near a rough surface the turbulence intensities are expected to be higher than for a smooth surface and therefore the instantaneous velocity vector has larger angular excursions. Perry *et al.* (1987) reported large differences in $-\overline{uv}$ in the boundary layer over an expanded mesh surface using ×-wire probes having 90° and 120° apex angles. The difference, which extended throughout the boundary layer, was of the order of 18% at $y/\delta = 0.1$. Since the difference was reduced considerably by flying the probes and the results for the flown 120° probe were essentially the same as those for the stationary 120° probe, the difference was attributed to an insufficient angular response for the 90° probe.

Acharya & Escudier (1987), using similar probes on a similar surface, reported a strong effect on $\overline{v^2}$, but found little effect on $-\overline{uv}$. Also, their U_τ extrapolated from the $-\overline{uv}$ profiles agreed with their drag balance to within a few percent for both probes.

In this experiment probe angles ranging from 95° to 140° were used, although the majority of the data were obtained with apex angles of about 125°. Results for $\overline{u^2}$, $\overline{v^2}$ and $-\overline{uv}$ are shown in figure 3. The data have been scaled with the average value of U_τ from all measurements obtained by extrapolating $-\overline{uv}$ to the wall. This value is $U_\tau = 1.0$ m/s which is 4% lower than the average value obtained from the curve fit of the mean profiles and corresponds to $C_f = 5.0 \times 10^{-3}$. Also included are the data obtained by Acharya & Escudier using 5 μm wire probes with 90° and 120° apex angles.

As shown in figure 3(*a*), the scatter in $\overline{u^2}$ is small and the results from the different

×-wire probes agree well with the data obtained using single normal wires (not shown). Although very similar, the rough-wall data are seen to be consistently slightly higher than for the smooth wall. The same was found by Perry & Li (1990) who attributed this to the stronger wake in the rough case. The present results are slightly higher close to the wall than the data of Acharya & Escudier, possibly because the wires used in this experiment were much shorter. Their probes were fully etched with a length to wire diameter ratio of $l_w/d_w = 250$. The present 5 μm diameter wire probes had apex angles of 95° and 129° and were partly etched, with $l_w/d_w = 140$.

The large effect of apex angle on $\overline{v^2}$ found by Acharya & Escudier through most of the boundary layer was not found in the present experiment, as may be seen in figure 3(*b*). The present data support their 120° probe data. Only in the region $y/\delta \lesssim 0.3$ are the measurements from the present 95° probe lower than for the 129° probe. The difference increases as the wall is approached, which is to be expected if the problem is due to the limited angular response, since the range of flow angles is only large near the surface.

Except where the apex angle limitations of the 95° probe are felt, the data from all probes (except for the 1.3 μm wire probe) are in close agreement. The measurements from the finer wire probe produces values for $(\overline{v^2})^{\frac{1}{2}}$ which are about 6% higher than the rest, except very close to the surface ($y < 2.5k$) where effects of streamwise positioning differences may be present. However, the sensor length for the 1.3 μm probe was only 0.3 mm compared with $l_w = 0.6$ and 0.7 mm for the 2.5 and 5 μm probes respectively. It is therefore possible that the higher $(\overline{v^2})^{\frac{1}{2}}$ values obtained with the 1.3 μm probe reflects the better fine-scale resolution of this probe. It would appear that the effect of sensor length may be just as important to the correct measurement of v as the probe apex angle. The effect of wire length on $\overline{u^2}$ as measured with a single hot wire was shown by Ligrani & Moffat (1986) to be important in the inner region of a rough-wall boundary layer. It would be useful to investigate the effect of wire length on $\overline{v^2}$ further.

Although the shear stresses measured with the 95° and 129° probes differ somewhat, the differences are only about half of those reported by Perry *et al.* (1987).

To investigate further the effect of limited angular resolution, the fractional contributions to $\overline{u^2}$, $\overline{v^2}$ and $\overline{uv}$ have been plotted in figure 4 in terms of the instantaneous flow angles. This contribution has been defined as

$$P_f(\gamma) = \lim_{T\to\infty} \frac{1}{\Delta\phi \bar{f} T} \int_0^T f I_1(t,\gamma)\,\mathrm{d}t,$$

where $f \equiv u^2$, v^2 or uv. The indicator function $I_1(t,\gamma)$ is defined as

$$I_1(t,\gamma) = \begin{cases} 1 & \text{if } \phi - \tfrac{1}{2}\Delta\phi \leqslant \gamma < \phi + \tfrac{1}{2}\Delta\phi \\ 0 & \text{otherwise,} \end{cases}$$

so that f is limited to the occurrences when the flow angle γ is within the range $\Delta\phi$ centred on ϕ. $\bar{f}$ is the conventional time average of f so that $\int_{-\infty}^{\infty} P_f(\gamma)\,\mathrm{d}\gamma = 1$.

The distribution of P_f provides more useful information about the effect of limited angular response than the probability density function used by Perry *et al.* While the p.d.f. gives the probability of the flow vector pointing at a certain angle, it can only answer the question of whether the probe angle is large enough to capture the full range of angles. The fractional contribution indicates how significant any limitation in the geometry is with respect to the quantity that is being measured.

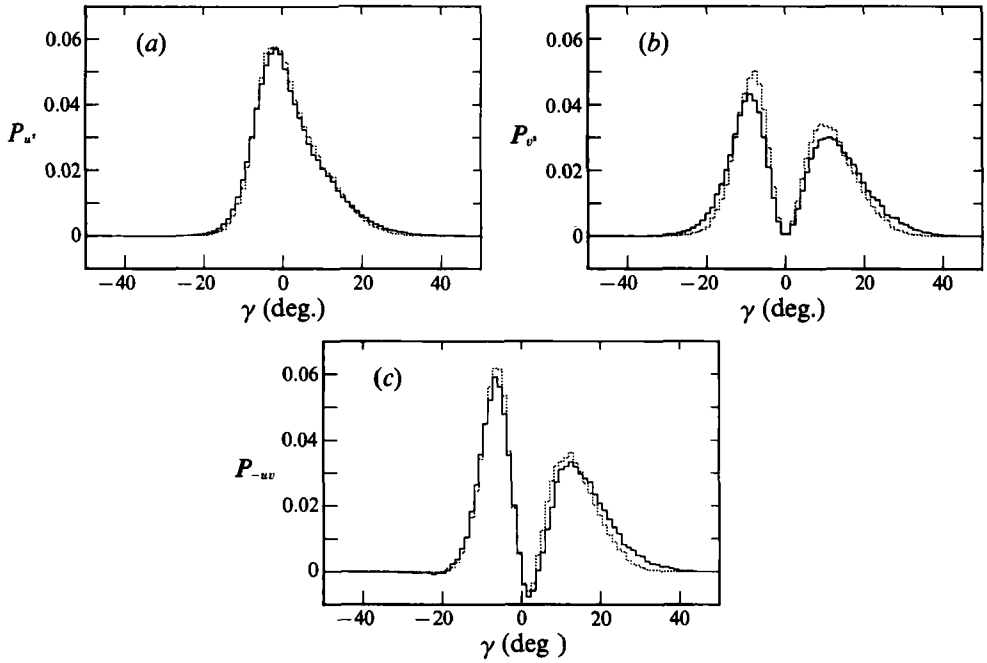

FIGURE 4. Contributions to Reynolds stresses at $y/\delta = 0.1$ as a function of the instantaneous flow angle: (*a*) u^2; (*b*) v^2; (*c*) $-uv$. ——, 5 μm × -wire probe with 129° apex angle; - - -, 5 μm × -wire probe with 95° apex angle.

A comparison has been made at $y/\delta = 0.1$ between measurements from the 95° and 129° probes. The two distributions of P_{u^2} in figure 4(*a*) are almost identical and show that most of the contribution comes from a narrow band in the region $|\gamma| < 10°$. Since flow angles larger than 20° contribute very little to $\overline{u^2}$, this explains why the measured $\overline{u^2}$ is virtually insensitive to the probe geometry.

As expected, the distribution for v^2 shown in figure 4(*b*) is bimodal, since there are no contributions to v^2 when $\gamma = 0$. While the contribution to u^2 was limited to $|\gamma| < 10°$, v^2 receives its major contributions near $\gamma = \pm 10°$. Also the distribution is skewed towards positive angles which implies that strong outward motions contribute more to v^2 than motions towards the surface. Because of the larger contributions at higher flow angles, the measurement of v^2 should be more sensitive to the probe apex angle than that of u^2. P_{v^2} is smaller for the 95° than the 129° probe in the region $|\gamma| > 15°$. It therefore appears that measurement errors due to limited probe apex angles begins to influence the data at flow angles which are considerably smaller than half the apex angle. This is in agreement with the findings of Perry *et al.*, but the effect this has on $\overline{v^2}$ was not found to be as severe in this experiment as reported by Acharya & Escudier.

Since P_{u^2} is not very sensitive to probe geometry and receives little contribution at larger angles, the distributions of P_{uv}, shown in figure 4(*c*), must be expected to be less sensitive than P_{v^2} since P_{uv} relies on the correlation between u and v. Consequently the difference in U_τ found by extrapolating the $\overline{uv}$ distributions to the wall for the 95° and 129° probes was only about 3%. This is more consistent with the findings of Acharya & Escudier than the large effect reported by Perry *et al.*

The present measurements of $\overline{uv}$ for the rough wall are in close agreement (figure 5) with the distribution of $\overline{uv}$ calculated using the x-momentum equation and the

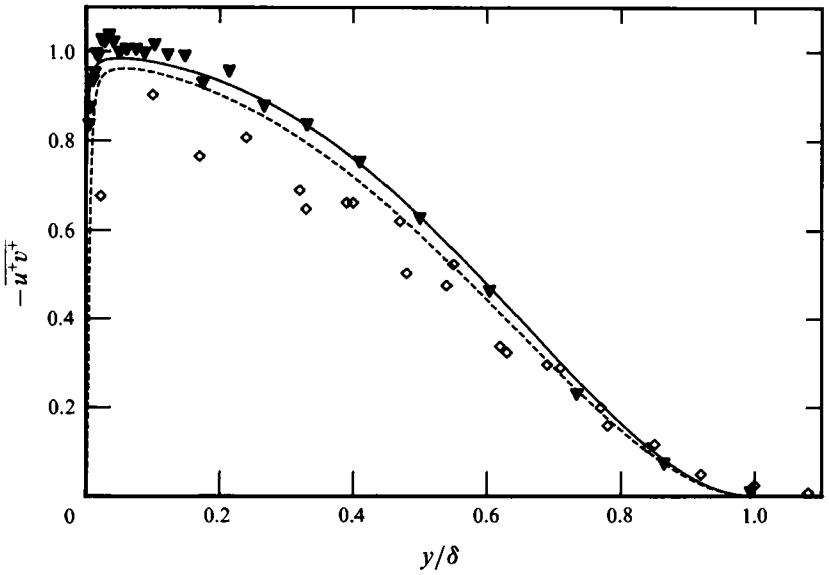

FIGURE 5. Comparison between measured Reynolds shear stress distributions and calculations using the mean momentum equation. Calculation: ——, smooth wall ($R_\theta = 6030$); ——, rough wall ($R_\theta = 12800$). Measurements: symbols as in figure 1.

measured mean velocity distribution. The agreement between measured and calculated $\overline{uv}$ distributions for the smooth-wall boundary layer is also reasonable, except in the inner region of the layer. For the calculation of $\overline{uv}$, a similarity form of the mean velocity profile, fully consistent with (1) and (7), as adopted by Granville (1988) was used. This leads to a relatively simple algebraic expression for the total shear stress from which the Reynolds shear stress can be inferred after subtracting the viscous shear stress.

5. Quadrant decomposition

A useful way of quantifying possible differences between smooth- and rough-wall boundary layers is to compare the contributions to $\overline{uv}$ from the main quadrants (Q2 and Q4) in these two flows. The u–v quadrant decomposition technique has been effective for assessing the importance of visually observed ejections and sweeps in the wall region of boundary layer and duct flows (Wallace, Eckelmann & Brodkey 1972; Willmarth & Lu 1972). More generally, it has enabled the importance of Q2 and Q4 motions, of particular strengths, to be evaluated across the whole flow. Using Lu & Willmarth's (1973) concept of a hyperbolic hole of size H, defined by $|uv| = Hu'v'$ (a prime denotes an r.m.s. value), the contribution to $\overline{uv}$ from a particular quadrant can be written as

$$(\overline{uv})_Q = \lim_{T\to\infty} \frac{1}{T} \int_0^T uvI_2(t)\,\mathrm{d}t,$$

where I_2 is an indicator function defined so that

$$I_2 = \begin{cases} 1 & \text{when } |uv|_Q \geqslant Hu'v' \\ 0 & \text{otherwise.} \end{cases}$$

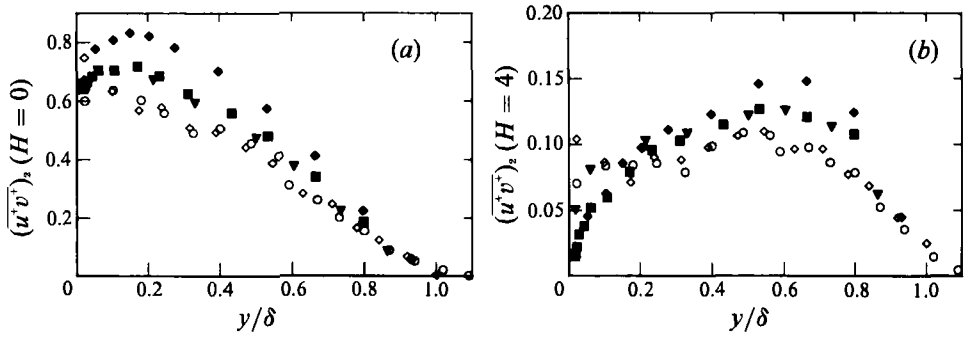

FIGURE 6. Contribution to $\overline{u^+v^+}$ from quadrant 2. (*a*) $H = 0$; (*b*) $H = 4$. Symbols are as in figures 1 and 3.

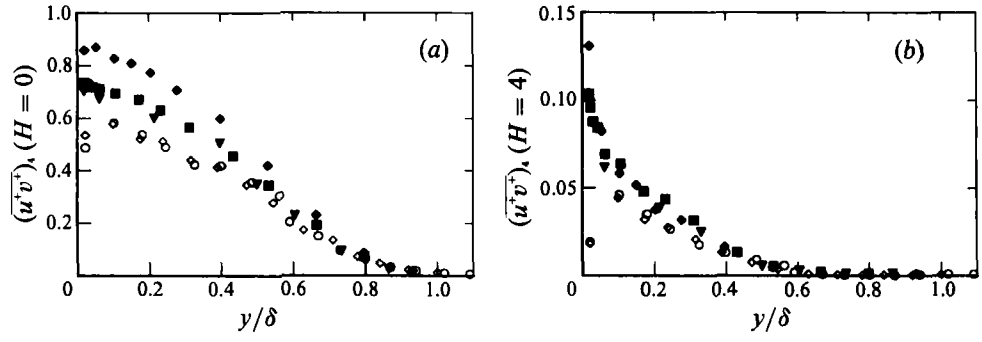

FIGURE 7. Contribution to $\overline{u^+v^+}$ from quadrant 4. (*a*) $H = 0$; (*b*) $H = 4$. Symbols are as in figures 1 and 3.

As the main interest here is in quadrants 2 and 4, results are presented only for $Q = 2$ and $Q = 4$.

Distributions of $(\overline{u^+v^+})_2$, shown in figure 6(*a*) for $H = 0$, indicate that, for most of the boundary layer, its magnitude is larger on the rough wall than on the smooth wall. This observation also applies for $y/\delta \gtrsim 0.2$ when only strong events ($H = 4$) are selected (figure 6*b*), but for $y/\delta \lesssim 0.2$, $(\overline{u^+v^+})_2$ is larger over the smooth wall than over the rough wall.

In the wall region, the magnitude of $(\overline{u^+v^+})_4$ is significantly larger for the rough wall than for the smooth wall when $H = 0$ (figure 7*a*). This difference slowly decreases as y/δ increases, and is negligible at the edge of the layer. The near-wall difference in $(\overline{u^+v^+})_4$ between rough and smooth walls is amplified when H is increased (figure 7*b*). In this case however, the smooth- and rough-wall distributions are nearly identical for $y/\delta \gtrsim 0.2$.

The results of figures 6(*b*) and 7(*b*) underline an important difference between the smooth- and rough-wall layers. In the outer regions, strong Q2 events make a larger contribution to $\overline{uv}$ in the rough-wall layer. By contrast, the inner region of the rough-wall layer is dominated by strong Q4 events (e.g. Nakagawa & Nezu 1977; Raupach 1981), presumably because the damping of v is less severe due to the open nature of the rough surface.

The ratio $\alpha = (\overline{uv})_2/(\overline{uv})_4$ was interpreted by Lu & Willmarth (1973) as a measure of the relative importance of Q2 and Q4 motions. This ratio was used by Teitel & Antonia (1991) to highlight differences in the outer regions of turbulent boundary layer and channel flows. For $H = 0$, figure 8(*a*) indicates that there are small

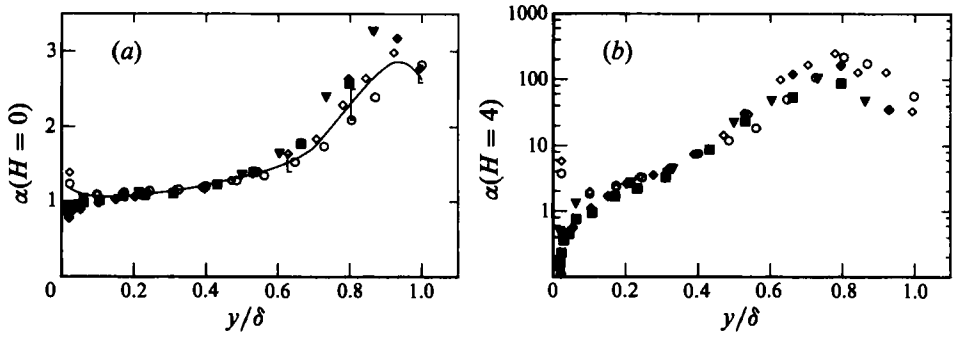

FIGURE 8. Ratio of contributions to $\overline{uv}$ from quadrants 2 and 4. (*a*) $H = 0$; (*b*) $H = 4$. Symbols are as in figures 1 and 3. ——, *d*-type rough wall, Osaka & Mochizuki (1988), $800 \leqslant R_\theta \leqslant 5000$.

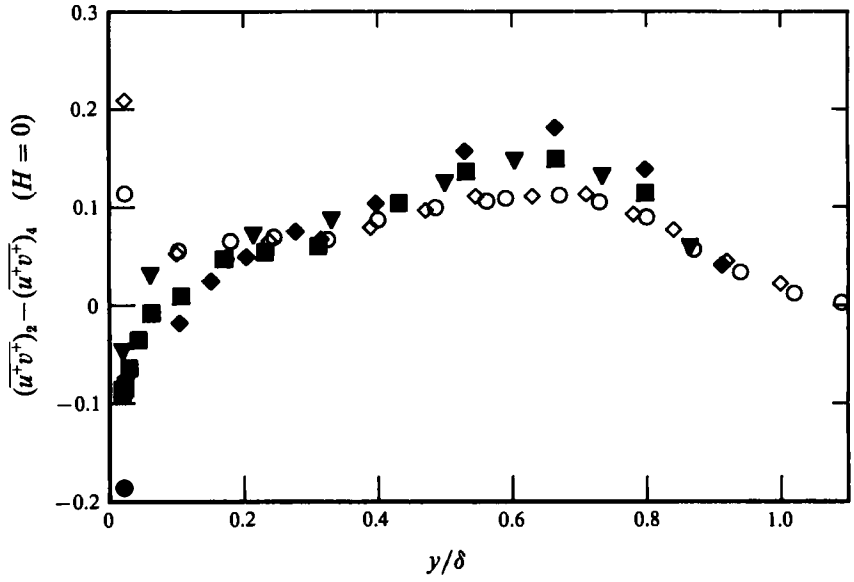

FIGURE 9. Difference between contributions from quadrants 2 and 4 to $\overline{u^+v^+}$. $H = 0$. Symbols are as in figures 1 and 3.

differences between the present rough-wall and smooth-wall values in the regions $y/\delta \lesssim 0.2$ and $y/\delta \gtrsim 0.6$. In the former region, the smaller value of the ratio near the rough wall reflects the importance of the sweep motion, while in the latter region the ratio is greater in the rough-wall layer emphasizing the generally greater strength of Q2 motions. The use of $H = 4$ emphasizes the differences in α close to the wall (figure 8*b*).

For interest, the distributions of $(\overline{uv})_2/(\overline{uv})_4$ measured in a *d*-type rough-wall boundary layer by Osaka & Mochizuki (1988) is also shown in figure 8(*a*). Allowing for the scatter (shown by the vertical bars) in the latter data, this distribution is practically the same over a wide Reynolds-number range ($800 \leqslant R_\theta \leqslant 5000$), indicating that Reynolds-number similarity may be achieved at a relatively small R_θ in a rough-wall boundary layer. The present (relatively high R_θ) smooth-wall distributions of $(\overline{uv})_2/(\overline{uv})_4$ are in reasonable agreement with the *d*-type rough-wall distribution, apparently reflecting the general similarity that may be expected between *d*-type rough-wall and smooth-wall boundary layers. Osaka & Mochizuki

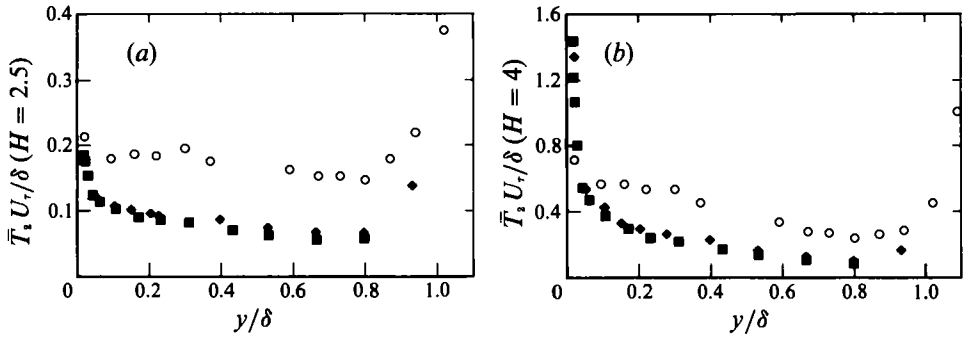

FIGURE 10. Average time between upward crossings ($|uv| > Hu'v'$) in quadrant 2. (*a*) $H = 2.5$, (*b*) $H = 4$. Symbols are as in figures 1 and 3.

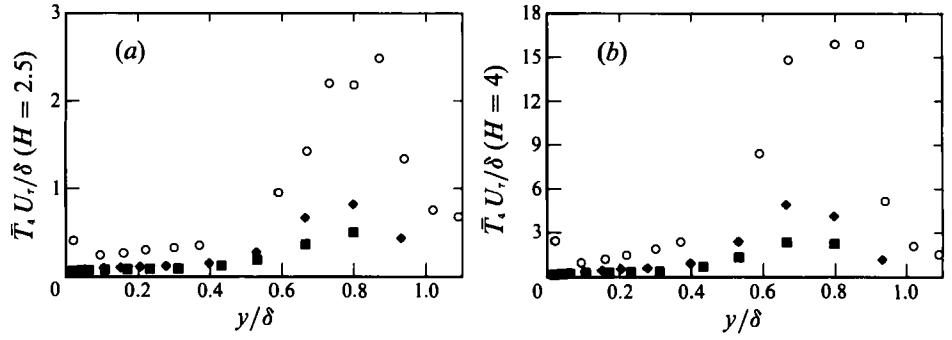

FIGURE 11. Average time between upward crossings ($|uv| > Hu'v'$) in quadrant 4. (*a*) $H = 2.5$; (*b*) $H = 4.0$. Symbols are as in figures 1 and 3.

did however report differences both in the mean velocity and turbulence intensities between their *d*-type rough-wall boundary layer and a smooth wall. Townsend (1976) noted that large-scale pressure fluctuations can lead to simultaneous ejections of the stagnant fluid (in the cavities between consecutive roughness elements) over areas comparable to the flow width, thus implying an ejection mechanism which may be different from that on a smooth wall. It is possible that differences between these two layers are detectable in the ratio $(\overline{uv})_2/(\overline{uv})_4$ for $H = 4$; however, this information is not available in Osaka & Mochizuki's paper.

Raupach (1981) found that a close correlation exists between the ratio $[(\overline{uv})_2 - (\overline{uv})_4]/\overline{uv}$ and the skewnesses of u and v, almost everywhere in the flow (independently of the nature of the surface). The present distributions of $(\overline{u^+v^+})_2$ and $(\overline{u^+v^+})_4$ indicate that $[(\overline{u^+v^+})_2 - (\overline{u^+v^+})_4]$ would not be the same for smooth and rough walls. Figure 9 shows that there are indeed differences between the two surfaces in both inner and outer regions (only results for $H = 0$ are shown as the dependence of $[(\overline{u^+v^+})_2 - (\overline{u^+v^+})_4]$ on H is not significant).

Lu & Willmarth and Raupach examined the variation across smooth-wall and rough-wall boundary layers of timescales associated with either ejections or sweeps of a certain strength. Here, we define $\bar{T}_2$ as the average time between consecutive upward crossings in quadrant 2 of a particular level $H = |uv|/u'v'$. Similarly, $\bar{T}_4$ is the average time between consecutive upward crossings in quadrant 4. Distributions of $\bar{T}_2 U_\tau/\delta$ across the boundary layer are shown in figures 10(*a*) and 10(*b*) for $H = 2.5$ and 4 respectively. The variation of $\bar{T}_4 U_\tau/\delta$ with y/δ is given in figures 11(*a*) and 11(*b*). It is clear, as noted previously by Lu & Willmarch and Raupach, that the

magnitudes of $\bar{T}_2 U_\tau/\delta$ and $\bar{T}_4 U_\tau/\delta$ depend critically on the value of H. Raupach found that when H was equal to about 1.6 (in Raupach's paper, H was defined as $|uv|/\overline{uv}$ and therefore differs from the present definition by a factor equal to ρ_{uv}, the correlation coefficient of u and v), $\bar{T}_2 U_\tau/\delta$ was approximately constant (≈ 0.13) over a significant fraction of the layer. The present smooth-wall value of $\bar{T}_2 U_\tau/\delta$ (≈ 0.19 for $H = 2.5$, figure 10*a*) is consistent with that of Raupach, after allowing for the slightly different values of H. The present rough-wall values of $\bar{T}_2 U_\tau/\delta$ (figure 10) are smaller than those on the smooth wall by a factor of almost two. This result does not support Raupach's conclusion that the magnitude of $\bar{T}_2 U_\tau/\delta$ is independent of surface roughness. The present experiments indicate that not only are Q2 events (over a significant part of the outer region) stronger for a rough-wall boundary layer but they also occur more frequently.

For $H = 4$, the magnitude of $\bar{T}_2 U_\tau/\delta$ increases near the wall, especially in the vicinity of the roughness. The scarcity of ejections near the roughness elements is consistent with the dominance of sweeps in this region. The distributions of $\bar{T}_4 U_\tau/\delta$ (figures 11*a*, *b*) are very similar to those presented by Raupach, with a peak occurring near $y/\delta \approx 0.7$. In the present case however, the magnitude of this peak is significantly smaller for the rough than for the smooth wall. Although Q4 events are rather infrequent near the outer edge of the layer, they occur relatively more frequently in the rough-wall layer, consistent with the higher frequency of Q2 events.

6. Spectra

In view of the previously noted differences, relative to the smooth wall, in the distributions of the Reynolds stresses (especially $\overline{v^2}$), it seems worthwhile to examine these differences in the spectral domain.

Spectra of u and v as well as uv co-spectra were calculated using a fast Fourier transform algorithm (averaged over an ensemble of 24 records, each including 2^{12} samples) at two locations in the layer (smooth and rough). At $y/\delta = 0.1$ (figure 12*a*), the normalizing scales for velocity and length are U_τ and y respectively. At $y/\delta = 0.4$ (figure 12*b*), U_τ and δ have been used. In both figures, the areas under the curves are given by

$$\int_0^\infty \phi_u \, \mathrm{d}k_1 = \overline{u^{+2}}, \quad \int_0^\infty \phi_v \, \mathrm{d}k_1 = \overline{v^{+2}}, \quad \int_0^\infty Co_{uv} \, \mathrm{d}k_1 = -\overline{u^+ v^+},$$

where $k_1 (\equiv 2\pi f/\bar{U}$, f is the frequency, $\bar{U}$ is the local mean velocity) is the one-dimensional wavenumber. Only small differences between the smooth and rough walls can be seen in the case of ϕ_u and Co_{uv}. At $y/\delta = 0.1$ the difference in ϕ_u occurs mainly for $k_1 y \lesssim 0.1$ and $k_1 y > 4$. The main difference in Co_{uv} occurs at wavenumbers for which Co_{uv} is maximum; the magnitude of Co_{uv} being slightly higher over the rough wall. This increase is consistent with the slightly larger values of $\overline{u^+ v^+}$ in the rough-wall layer. The major difference between rough and smooth walls is observed in ϕ_v, the difference being spread almost throughout the wavenumber range.

The trend of the distributions at $y/\delta = 0.4$ (figure 12*b*) is very similar to that at $y/\delta = 0.1$ (figure 12*a*), emphasizing that the spectral differences in v are maintained in the outer region of the layer.

The normalization in figure 12(*a*) is that used to distinguish between active and inactive motions (e.g. Bradshaw 1967). By definition, the active (or sometimes universal) motion contributes all of the Reynolds shear stress in the inner region. Townsend (1976) describes the inactive motion as a large-scale swirling motion in

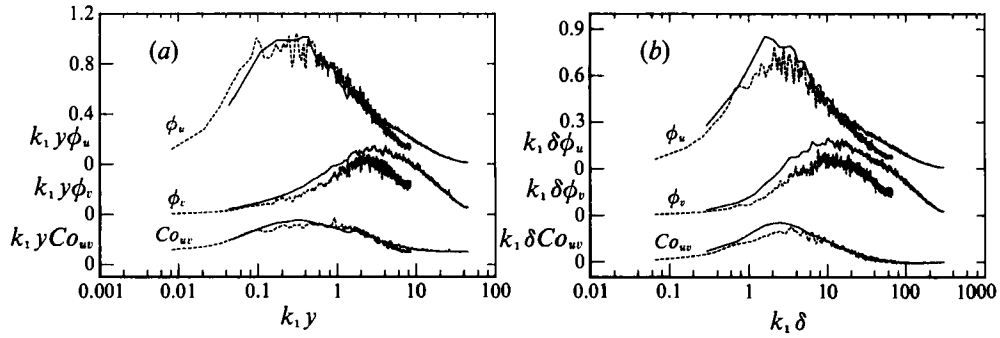

FIGURE 12. Spectra and co-spectra of u and v at two locations in the flow. (*a*) $y/\delta = 0.1$ (normalization is by y and U_τ); (*b*) $y/\delta = 0.4$ (normalization is by δ and U_τ): ——, rough surface (1.3 μm, 120° ×-wire with $l/d = 240$); – – –, smooth surface (5 μm, 90° ×-wire with $l/d = 250$).

planes parallel to the wall. This motion would contribute to $\overline{u^2}$ and $\overline{w^2}$ but not to $\overline{uv}$ or $\overline{v^2}$ (e.g. Perry *et al.* 1987). With a descriptive framework involving active and inactive motions only, the total contribution to v^{+2} would be from the active motion. In the (fully turbulent) inner region, the magnitude of v^{+2} (and indeed the normalized v-spectrum) would be expected to be flow-independent in the sense that the active motion is universal. The distributions in figures 12(*a*) and 12(*b*) suggest however that the active motion depends on the nature of the wall. It is also possible that the strength of the active motion may differ, especially in connection with $\overline{v^2}$, for different types of rough surfaces. It was suggested (Antonia *et al.* 1990) that the active motion is Reynolds-number dependent for a smooth-wall flow at low Reynolds numbers. It would seem therefore that the concept of a 'universal' active motion is strictly only an approximate one. The practical consequences of using this approximation are probably less serious for smooth-wall layers, where the magnitude of $\overline{v^2}$ is substantially smaller than for rough wall layers.

While the peaks in ϕ_u and Co_{uv} occur at approximately the same values of $k_1 y$, (≈ 0.2, 0.3 for $y/\delta = 0.1$) the peak in ϕ_v occurs at wavenumbers which are greater by one order of magnitude. This suggests that the setting for the filter cutoff frequency is more critical in the case of v than for u or w. The distributions of $k_1 y\phi_u$ and $k_1 yCo_{uv}$ in figure 12(*a*) have returned to zero at $k_1 y \approx 40$ (the filter cutoff frequency), the magnitude of $k_1 y\phi_v$ is small but not quite negligible at this wavenumber. The value of $k_1 y$ which corresponds to the filter cutoff frequency represents values of $k_1 \eta$ of about 0.38 at $y/\delta = 0.1$. (At $y/\delta = 0.4$, the filter cutoff setting corresponds to $k_1 \eta \approx 0.35$.) It would appear that a more satisfactory filter cutoff setting, from the point of view of capturing all of $\overline{v^2}$, would be $k_1 \eta \approx 0.5$. The failure to meet this (relatively stringent) requirement has caused $\overline{v^2}$ to be only slightly underestimated in the present experiment (by no more than 1%) at $y/\delta = 0.1$. It seems likely however that previously published values of $\overline{v^2}$ in rough-wall boundary layers may have been more seriously affected by this requirement.

7. Conclusions and discussion

Various measurements in a mesh screen rough-wall turbulent boundary layer have been compared with corresponding measurements in a smooth-wall layer at Reynolds numbers sufficiently large to satisfy Reynolds-number similarity. The roughness at the wall was shown to influence both the mean velocity profile and the turbulent

stresses well into the outer region of the boundary layer. This challenges the generally accepted idea that a k-type roughness only influences the flow structure in the immediate vicinity of the surface through the modified wall boundary condition. From an eddy shedding viewpoint, it appears plausible that the influence is felt well beyond the roughness layer. The eddies shed have a lengthscale proportional to the roughness scale k, a scale which in this experiment is significant compared to the turbulence scales expected in the outer layer. Owing to the less severe boundary restriction in the rough-wall case on the velocity component normal to the wall, the sweep or ejection velocities become stronger than for a smooth surface. This increased activity at the wall goes on continuously over the entire streamwise extent of the flow. Hence, when k is significant, the vortices shed will contribute to an increased intensity of turbulent motion and should therefore eventually also lead to a detectable change in the strength of the wake region (as discussed below).

The large difference between the wall shear stress value obtained by profile matching and the value derived by extrapolating the measured Reynolds stress profile to the wall which has been reported in previous rough-wall experiments, appears to be due to restrictions set by the frequently used velocity-defect formulation of Hama (1954). Rather than keeping the wake strength fixed at $\Pi = 0.52$ (the value which can be derived from Hama's formulation), Π was determined as part of the profile matching process. The resulting value of $\Pi (\approx 0.7)$ is greater than on a smooth wall ($\Pi \approx 0.5$ to 0.6), commensurate with the greater entrainment of irrotational fluid on a rough wall. The rough-wall shear stress derived in this way agrees well with the Reynolds shear stress extrapolated to the wall. The shear stress profile, derived from the streamwise momentum equation using the matched profile, agrees closely with the measurements. The incompatibility between the mean velocity and Reynolds stress profiles reported previously in the literature is absent in the present work.

The strong dependence of the $\times$-wire apex angle on $\overline{uv}$ reported by Perry *et al.* (1987) or on $\overline{v^2}$ found by Acharya & Escudier (1987) could not be verified in this experiment. Only close to the rough surface did probe limitations become apparent in $\overline{v^2}$. An inspection of how the contributions to $\overline{v^2}$ depend on flow angle showed that the reduced values measured by the probe with the smallest apex angle was associated with relatively large flow angles away from the wall.

There are only small differences in $\overline{u^{+2}}$ between smooth and rough walls. Only moderate differences are observed for $\overline{u^+v^+}$. However, the rough-wall distribution of $\overline{v^{+2}}$ is significantly larger than for the smooth wall, the increase being observed over the entire layer. A similar increase has been observed by Acharya & Escudier (1987) while a smaller increase was reported by Pimenta, Moffat & Kays (1975, 1979), these latter authors commenting that the effect of roughness on the turbulence structure extends well into the outer region.

In the wall region, contributions to $-\overline{u^+v^+}$ from the fourth quadrant in the (u, v)-plane is significantly greater for the rough wall than for the smooth wall, thus emphasizing the importance of sweeps near the roughness. The increased fourth-quadrant activity is made possible by the less severe boundary condition for v over the rough surface. It is conceivable that different roughness geometries will provide different constraints for v, e.g. crop canopies should not constrain v to the same degree as a closely packed sand-grain roughness. Although third-order v-based moments are not reported here, the data of Andreopoulos & Bradshaw (1981) and Bandyopadhyay & Watson (1988) indicate that such moments may provide a useful measure of this constraint. In the wall region, the contributions to $-\overline{u^+v^+}$ from

quadrant 2 are small by comparison to the region near the smooth wall. In the outer region, the contributions from quadrants 2 and 4 are noticeably larger in the rough-wall layer, consistent with the flow visualization observations of Grass (1971). Strong Q2 and Q4 events occur almost twice as frequently on the rough wall than on the smooth wall.

In Raupach's (1991) review of the turbulence structure in a rough-wall boundary layer, the main difference from a smooth-wall behaviour was assumed to be confined to a region near the roughness elements or roughness sublayer. Outside this region, smooth- and rough-wall boundary layers are assumed to have essentially the same structure. The present experiments, while confirming the expected departure in the vicinity of the roughness, indicate important departures from smooth-wall behaviour over a significant portion of the layer. This is at variance with the wall similarity hypothesis and suggests that the degree of interaction between the wall and the outer region may not be negligible. How these differences are reflected in the topology of the large-scale motion and how important this interaction is to the dynamics of the flow are matters which need to be investigated.

The rough-wall boundary condition is strongly evident in the increased magnitude of the v-spectrum, relative to the smooth wall. This increase is almost independent of wavenumber. It seems plausible that different roughnesses may have different spectral signatures for v. The variation in the v-spectrum when inner layer scaling is used suggests that the concept of a 'universal' active motion may need to be revised as new turbulence data on different types of rough surfaces become available.

REFERENCES

Acharya, M. & Escudier, M. 1987 Turbulent flow over mesh roughness. In *Turbulent Shear Flows 5* (ed. F. Durst, B. E. Launder, J. L. Lumley, F. W. Schmidt & J. H. Whitelaw), pp. 176–185. Springer.

Andreopoulos, J. & Bradshaw, P. 1981 Measurements of turbulence structure in the boundary layer on a rough surface. *Boundary-Layer Met.* **20**, 201–213.

Antonia, R. A., Bisset, D. K. & Browne, L. W. B. 1990 Effect of Reynolds number on the topology of the organised motion in a turbulent boundary layer. *J. Fluid Mech.* **213**, 267–286.

Bandyopadhyay, P. R. 1987 Rough-wall turbulent boundary layers in the transition regime. *J. Fluid Mech.* **180**, 231–266.

Bandyopadhyay, P. R. & Watson, R. D. 1988 Structure of rough-wall turbulent boundary layers. *Phys. Fluids* **31**, 1877–1883.

Bradshaw, P. 1967 Inactive motion and pressure fluctuations in turbulent boundary layers. *J. Fluid Mech.* **30**, 241–258.

Bradshaw, P. 1987 Wall flows. In *Turbulent Shear Flows 5* (ed. F. Durst, B. E. Launder, J. L. Lumley, F. W. Schmidt & J. H. Whitelaw), pp. 171–175. Springer.

Browne, L. W. B., Antonia, R. A. & Chua, L. P. 1989*a* Calibration of ×-probes for turbulent flow measurements. *Expts. Fluids* **7**, 201–208.

Browne, L. W. B., Antonia, R. A. & Chua, L. P. 1989*b* Velocity vector cone angle in turbulent flows. *Expts. Fluids* **8**, 13–16.

Clauser, F. H. 1956 The turbulent boundary layer. *Adv. Appl. Mech.* **4**, 1–51.

Coles, D. E. 1956 The law of the wake in the turbulent boundary layer. *J. Fluid Mech.* **1**, 191–226.

Coles, D. E. 1987 Coherent structures in turbulent boundary layers. In *Perspectives in Turbulence Studies* (ed. H. U. Meier & P. Bradshaw), pp. 93–114. Springer.

Finley, P. J., Khoo Chong Phoe & Chin Jeck Poh 1966 Velocity measurements in a thin turbulent wake layer. *La Houille Blanche* **21**, 713–721.

Furuya, Y. & Fujita, H. 1967 Turbulent boundary layers on a wire-screen roughness. *Bull JSME* **10**, 77–86.

GRANVILLE, P. S. 1976 A modified law of the wake for turbulent shear layers. *Trans. ASME* I: *J. Fluids Engng* **98**, 578–580.

GRANVILLE, P. S. 1988 Eddy viscosities and mixing lengths for turbulent boundary layers on flat plates, smooth or rough. *J. Ship Res.* **32**, 229–237.

GRASS, A. J. 1971 Structural features of turbulent flow over smooth and rough boundaries. *J. Fluid Mech.* **50**, 233–255.

HAMA, F. R. 1954 Boundary layer characteristics for smooth and rough surfaces. *Trans. Soc. Naval Archit. Mar. Engrs* **62**, 333–358.

KLEBANOFF, P. S. 1955 Characteristics of turbulence in a boundary layer with zero pressure gradient. *NACA Rep.* 1247.

KLINE, S. J. & ROBINSON, S. K. 1990 Quasi-coherent structures in the turbulent boundary layer. Part I: Status report on a community-wide summary of the data. In *Near-Wall Turbulence* (ed. S. J. Kline & N. H. Afgan), pp. 200–217. Hemisphere.

KROGSTAD, P.-Å. & BROWNE, L. W. B. 1991 Turbulent boundary layer flow over a rough surface. *Rep.* TN-FM 91/1. Department of Mechanical Engineering, University of Newcastle, NSW.

LIGRANI, P. M. & MOFFAT, R. J. 1986 Structure of transitionally rough and fully rough turbulent boundary layers. *J. Fluid Mech.* **162**, 69–98.

LU, S. S. & WILLMARTH, W. W. 1973 Measurements of the structure of the Reynolds stress in a turbulent boundary layer. *J. Fluid Mech.* **60**, 481–571.

NAKAGAWA, H. & NEZU, I. 1977 Prediction of the contributions to the Reynolds stress from bursting events in open-channel flows. *J. Fluid Mech.* **80**, 99–128.

OSAKA, H. & MOCHIZUKI, S. 1988 Coherent structure of a *d*-type rough wall boundary layer. In *Transport Phenomena in Turbulent Flows: Theory, Experiment and Numerical simulation* (ed. M. Hirata & N. Kasagi), pp. 199–211. Hemisphere.

PERRY, A. E. & ABELL, C. J. 1977 Asymptotic similarity of turbulence structures in smooth- and rough-walled pipes. *J. Fluid Mech.* **79**, 785–799.

PERRY, A. E. & LI, J. D. 1990 Experimental support for the attached-eddy hypothesis in zero-pressure-gradient turbulent boundary layers. *J. Fluid Mech.* **218**, 405–438.

PERRY, A. E., LIM, K. L. & HENBEST, S. M. 1987 An experimental study of the turbulence structure in smooth- and rough-wall boundary layers. *J. Fluid Mech.* **177**, 437–466.

PIMENTA, M. M., MOFFAT, R. J. & KAYS, W. M. 1975 The turbulent boundary layer: an experimental study of the transport of momentum and heat with the effect of roughness, *Rep.* HMT-21. Thermosciences Division, Stanford University.

PIMENTA, M. M., MOFFAT, R. J. & KAYS, W. M. 1979 The structure of a boundary layer on a rough wall with blowing and heat transfer. *Trans. ASME* C: *J. Heat Transfer* **101**, 193–198.

RAUPACH, M. R. 1981 Conditional statistics of Reynolds stress in rough-wall and smooth-wall turbulent boundary layers. *J. Fluid Mech.* **108**, 363–382.

RAUPACH, M. R., ANTONIA, R. A. & RAJAGOPALAN, S. 1991 Rough-wall turbulent boundary layers. *Appl. Mech. Rev.* **44**, 1–25.

SABOT, J., SALEH, I. & COMTE-BELLOT, G. 1977 Effect of roughness on the intermittent maintenance of Reynolds shear stress in pipe flow. *Phys. Fluids* **20**, S150–S155.

TANI, I. 1988 Turbulent boundary layer development over rough surfaces. In *Perspectives in Turbulence Studies* (ed. H. U. Meier & P. Bradshaw), pp. 223–249. Springer.

TANI, I., MUNAKATA, H., MATSUMOTO, A. & ABE, K. 1988 Turbulence management by groove roughness. In *Turbulence Management and Relaminarisation* (ed. H. W. Liepmann & R. Narasimha), pp. 161–172. Springer.

TEITEL, M. & ANTONIA, R. A. 1991 Comparison between a turbulent boundary layer and a turbulent duct flow. *Expts. Fluids* **11**, 203–204.

TOWNSEND, A. A. 1976 *The Structure of Turbulent Shear Flow.* Cambridge University Press.

WALLACE, J. M., ECKELMANN, H. & BRODKEY, R. S. 1972 The wall region in turbulent shear flow. *J. Fluid Mech.* **54**, 39–48.

WILLMARTH, W. W. & LU, S. S. 1972 Structure of the Reynolds stress near the wall. *J. Fluid Mech.* **55**, 65–92.